Experimental Investigations on Seismic Behavior and Design of Bottom Boundary Column in Steel Plate Shear Walls

Chao-Hsien Li
National Center for Research on Earthquake Engineering, Taiwan (R.O.C.)

Hung-Chi Lee & Keh-Chyuan Tsai
National Taiwan University, Taiwan (R.O.C.)

Chih-Han Lin
National Center for Research on Earthquake Engineering, Taiwan (R.O.C.)

SUMMARY:
This study proposes a series of capacity design procedures to determine the flexural or shear demands for the bottom boundary column in steel plate shear wall (SPSW). The proposed design requirement is to prevent the formation of the plastic hinge at the column top end. Three full-scale two-story SPSW were cyclically tested up to a roof drift of 4.5% rad. at Taiwan National Center for Research on Earthquake Engineering in 2011. All the specimens have the same infill plates and boundary beams. The key difference among the specimens is the member size of the boundary column. Test results confirm that the proposed design methods can effectively predict the occurrence of the flexural or shear plastic hinge at the top end of the bottom column. Test results show that the formation of the top-end plastic hinge in the bottom column in SPSWs would lead to a soft-story mechanism or instability problem.

Keywords: steel plate shear wall (SPSW), capacity design, seismic design, boundary column

1. INTRODUCTION

Steel plate shear wall (SPSW) is a cost-effective lateral force resisting system of the building structures. This system has been increasingly used in the Japan and North American in the recent years. An SPSW consists of infill steel plates and a boundary frame (Fig. 1.1a). In the current U.S. seismic provisions (AISC, 2010), the boundary beams and columns surrounding the infill plates are denoted horizontal boundary elements (HBE) and vertical boundary elements (VBE), respectively. SPSWs can effectively resist earthquake forces by allowing the unstiffened thin infill plates buckling in shear and developing the tension field action. The seismic input energy is then dissipated through the cyclic yielding of the infill plates in tension. The concept of using the post-buckling strength of the steel plate was first proposed by Thorburn *et al.* (1983). In their research, a strip model (Fig. 1.1b) and an equivalent brace (EB) model (Fig. 1.1c) were developed. The strip model uses at least 10 inclined truss members pin-connected to the columns and beams to represent the tension field action of a steel plate. The method for estimating the angle α of the tension field action has been developed (Timler and Kulak 1983). The EB model assumes that all tension strips develop equal strain and can be replaced by a single diagonal truss member pin-connected at the two ends to the supporting frame.

In the recent years, several researches explored the capacity design methods for the boundary elements. Park *et al.* (2007) proposed a simplified method for estimating the axial and flexural demands on the columns. Their method only considers the force demands induced from the plastic tension field forces of the infill panels without the actions from the swaying of the boundary element frame. Berman and Bruneau (2008) proposed a design method for calculating the ultimate column axial and flexural demands for SPSWs with pin-supported column bases. This method was developed based on their previous study of the plastic analysis methods for SPSWs (Berman and Bruneau 2003). Vian *et al*. (2009) developed the capacity design for the boundary beams at the top level of an SPSW to avoid the formation of the plastic hinge within the span of the top beam. Qu and Bruneau (2010a) explored the design procedure for the intermediate boundary beam. Qu and Bruneau (2010b) proposed the design methods to prevent the shear yielding and out-of-plane buckling of the boundary column.

The research team in National Center for Research on Earthquake Engineering (NCREE) focused on the seismic behaviour and design for the bottom boundary column. Tsai *et al*. (2010) proposed the capacity design method to limit the plastic hinge in the bottom boundary column at the column bottom end. Subsequently, Li *et al*. (2012) proposed a less-stringent design method to ensure the plastic hinge forming within the bottom quarter height of the bottom boundary column. This study aims at further cost-effective designs for the bottom boundary column. This study proposes the design requirement to prevent the formation of the plastic hinge at the column top end under various deformation levels of the SPSW. In order to verify the effectiveness of the proposed design methods, three full-scale two-story SPSW were cyclically tested up to a roof drift of 4.5% rad. at NCREE in 2011. This paper introduces the proposed capacity design methods and present the test results.

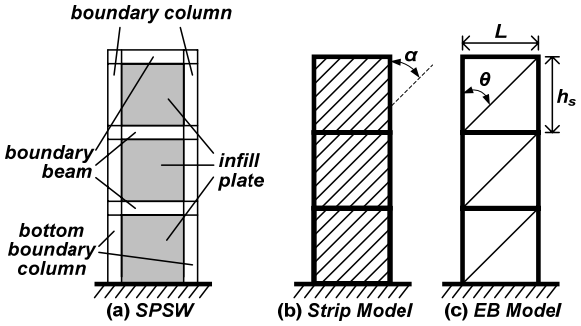

Figure 1.1. Schematics of (a) SPSW; (b) strip model and (c) EB model

2. CAPACITY DESIGN FOR BOTTOM BOUNDARY COLUMN IN THE SPSW

2.1. Pushover responses of an SPSW

Based on observations in the past SPSW tests, Fig. 2.1 illustrates the pushover response of an SPSW incorporating proper seismic design. The responses can be summarized into five sequential limit states:

(1) State-E (Elastic): The whole SPSW must remain elastic when the structure is subjected to the code prescribed seismic forces.
(2) State-PIY (Plates Initially Yield): State-PIY is defined as the state when the infill plates first experience yielding near the tensile diagonal region and the boundary elements remain elastic in this state. The story drift is about 0.3~0.5% rad. in this state.
(3) State-FSY (Frame Significantly Yield): As the story drift reaches approximately 0.5~0.75% rad., significant yielding of the whole structure is observed. Except for the corner regions of the infill plates, the majority part of the infill plates has yielded. In addition, some beam ends form plastic hinges at this stage.
(4) State-UYM (Uniform Yielding Mechanism): SPSW develops a uniform yielding mechanism (Berman and Bruneau, 2003) when the story drift is around 1% rad. All the infill plates develop the plastic tension field action and the plastic hinges form at the beam ends and the column bases.
(5) State-MCE (Maximum Considered Earthquake): State-MCE is the state when the deformation of an SPSW reaches the peak value that an SPSW would suffer during a MCE. Coinciding with the model building code, the MCE is defined as an earthquake has 2% probability of exceedance within 50 years. At this state, the plastic zones which had fully-developed at the State-UYM have experienced strain-hardening. The remaining parts except for those plastic zones should be designed to remain essentially elastic at this state in order to avoid the occurrence of any undesirable plastic mechanism. The past test (Qu, *et al.*, 2008) suggests that the peak inter-story drift of a properly-designed 2-story SPSW during MCE ground motions would reach about 2.5% rad. Thus, this research proposes that the representative story drift for State-MCE is 2.5% rad.

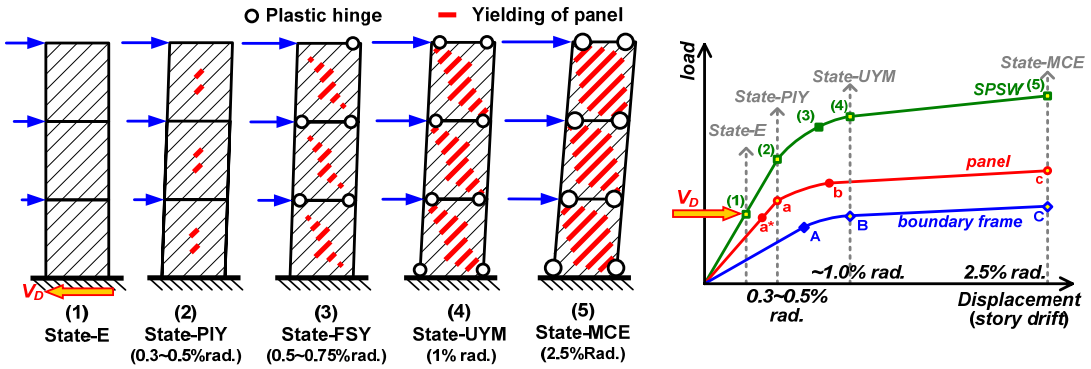

Figure 2.1. Pushover responses of well-designed SPSWs

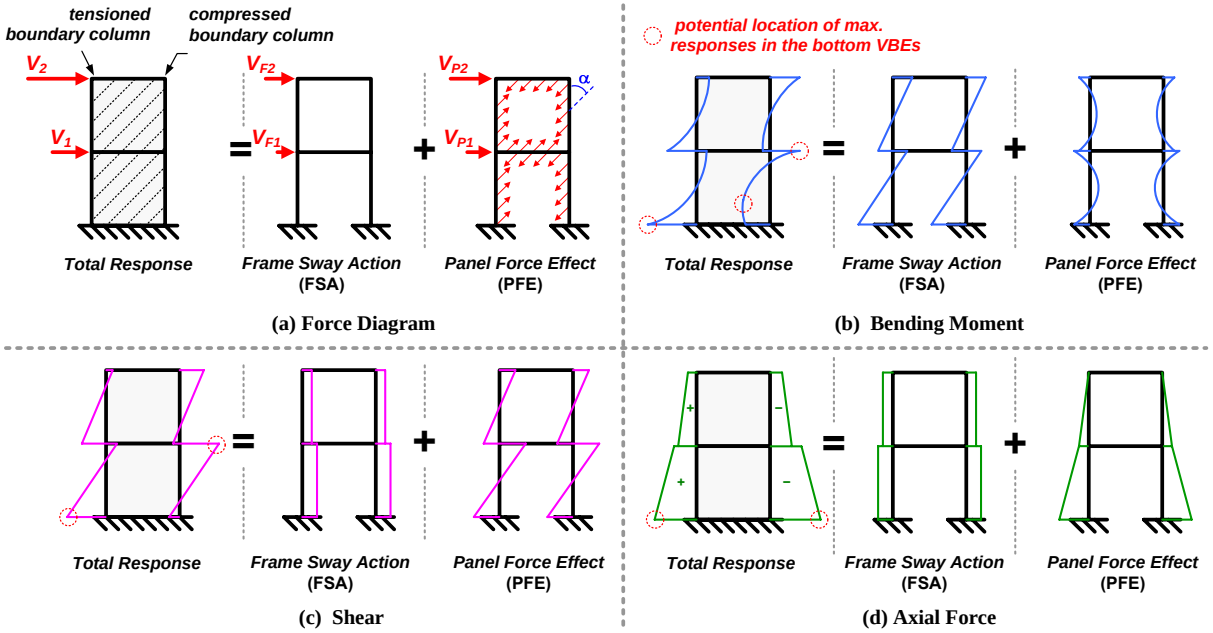

Figure 2.2. Superposition method for estimating the actions in the boundary column: (a) force diagrams (b) bending moment diagrams; (c) shear diagrams and (d) axial force diagrams

2.2. Superposition method for estimating the actions in boundary elements

As illustrated in Fig 2.2a, past researches (Vian and Bruneau, 2005; Tsai *et al.*, 2010; Li *et al.*, 2012) proposed that the actions of the boundary elements in an SPSW subjected to lateral forces can be estimated by superposing the actions due to "*frame sway action* (FSA)" and "*panel force effect* (PFE)". FSA is the action induced from the sway of the boundary frame; PFE is the effect due to the tension field force of the infill plates acting on the boundary frame. As the infill plates develop the tension field action under lateral forces, the panel forces acting on the boundary frame can be considered as distributed loads with an inclination angle, α (Timler and Kulak, 1983) to the vertical.

Figures 2.2b, 2.2c and 2.2d show the representative diagrams of the bending moments, shears and axial forces of the boundary columns in an SPSW subjected to the lateral forces. The locations where the maximum of the elastic member forces occur indicate the possible plastic zones in the boundary columns. As shown in Fig. 3b, the bending moments in the boundary elements due to the FSA and the PFE are assumed to be linear and quadratic functions, respectively. The shear forces induced by FSA and FE are supposed to be uniformly and linearly distributed. It should be noticed that, for the FSA bending moments in the bottom columns, the magnitude of the bottom-end moment is greater than the top end moment. This is because the rotational restraint at the fix-supported column base is larger than

that at the top end of the bottom column.

For the tensioned bottom boundary column, the flexural responses (shear force and bending moment) due to FSA and PFE are in the same direction at the bottom end but opposite at the top end. Thus, the maximum flexural responses occur at the bottom end (Figs. 2.2b and 2.2c). In addition, the maximum axial force occurs at the bottom end (Fig. 2.2d). The coincidence of the locations of the elastic maximum axial force, shear and bending moment indicates that the plastic zone in the tensioned bottom column will only form at the bottom end.

By contrast, the location of the potential plastic zone in the compressed bottom boundary column is not unique. The maximum values of the axial force, shear and bending moment in the compressed bottom column are not located at the same place. The maximum axial force is at the bottom end (Fig. 2.2d) while the maximum shear occurs at the top end (Fig. 2.2c). Furthermore, the curved shape of the moment diagram implicates the maximum bending moment possibly occurs at the top end or in the lower half of the column. Assuming the interaction between the shear and bending moment is negligible, three kinds of plastic behaviors could appear in the compressed bottom column: (1) shear plastic hinge at the top end; (2) flexural plastic hinge at the top end and (3) flexural plastic zone in the lower half of the column.

As the plastic zone in the compressed bottom column could be developed at various locations, the capacity design method for the bottom column shall focus on the compressed one. Specific capacity designs are required to avoid the formation of the undesired plastic hinge and to ensure the occurrence of the proper plastic mechanism. On the basis of the strong column/weak beam principle, the formation of the plastic hinge at the top ends of the bottom columns shall be avoided. Therefore, the objective of the proposed design method in this study aims at preventing the occurrence of the top-end plastic hinge in the compressed boundary column.

2.3. Proposed capacity design methods for bottom the boundary column

2.3.1. Method 1: Prevention of the top-end plastic hinge formation prior to the lower plastic hinge at State-UYM

Superposition method is used to estimate the bending moment of the compressed bottom column at the initiation of the State-UYM. As shown in Fig. 2.3, the bending moment due to FSA is assumed to be linearly-distributed. Assume that the bottom-end moment is λ times than top-end moment, M_f. As the rigidity of the fixed column base is larger than that at the column's top end, the λ value is greater than 1. Past research (Li *et al*., 2010) has validated that the λ value can be estimated from an elastic static frame analysis using the EB model.

The plastic tension field action of the bottom infill panel is expected to take place prior to the yielding of the bottom column. The bending moment due to the PFE can be computed from assuming both column ends are fixed and the column is subjected to a uniformly distributed load $\omega_{ch1}= R_y F_{yp} t_{p1} \sin\alpha^2$, which represents the horizontal component of the plastic tension field forces from the bottom panel. The R_y, F_{yp} and t_{p1} represent the material overstrength factor, yield stress and thickness of the infill plate at the bottom of the SPSW, respectively.

Superposing the bending moments due to FSA and PFE, the total bending moment distribution $M(y)$ of the compressed bottom column at the initiation of the plastic hinge formation can be estimated from:

$$M(y) = \underbrace{\lambda M_f \left(1 - \frac{1+\lambda}{\lambda h_1} y\right)}_{\text{frame sway action}} + \underbrace{\frac{\omega_{ch1}}{12}\left[-6y^2 + 6h_1 y - h_1^2\right]}_{\text{panel force effect}} \tag{2.1}$$

where h_1 is the height of the bottom VBE. It can be found there are two extreme values in this total bending moment distribution: one is in the lower half column height and the other is at the top end.

By solving the equation $M'(y) = 0$, the solution $y = y^*$ represents the location of the extreme moment within the lower half column height; and the $M(y^*)$ is the magnitude of the extreme moment. The magnitude of the top-end moment is $M_f + \omega_{ch1}h_1^2/12$. Assuming the within-height extreme moment $M(y^*)$ is equal to the plastic moment capacity of the column, M_p^* and the M_p^* is larger than the top-end moment, the required flexural strength of the column $M_{p\text{-}req}$ is obtained:

$$M_p^* > M_{p-req} = \left[\frac{\left(\lambda^2-4\lambda+19\right)+\sqrt{48\lambda^2-192\lambda+336}}{\left(1+\lambda\right)^2}\right]\omega_{ch1}h_1^2 = \eta_1\omega_{ch1}h_1^2 \tag{2.2}$$

When the reduced plastic moment of the bottom column, M_p^*, under the P-M interactions is greater than the $M_{p\text{-}req}$, it is guaranteed that the plastic hinge at the top end will not form prior to the formation of the plastic hinge in the lower half column height. From the conservative perspective, this study suggests that determination of M_p^* should consider the bottom-end axial force demand, P^b_d at state-UYM, even though the actual location of the plastic hinge could be above the bottom end. The axial demand P^b_d includes the axial forces due to the gravity load effect and the overturning action (as shown in the Fig 2.3b). The M_p^* can be determined from $1.18M_p(1\text{-}P^b_d/P_y)$ (AISC, 2005), where M_p and P_y are the plastic moment and yield axial strength of the column, respectively.

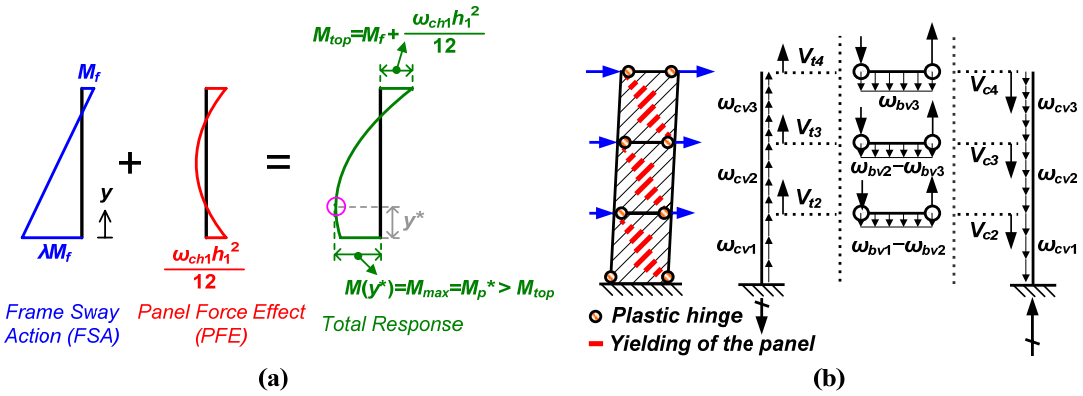

Figure 2.3. (a) Superposition method for estimating the bending moment in the compressed bottom column and (b) plastic mechanism of SPSW and force diagram for estimating the overturning axial forces in columns

2.3.2. Method 2: Prevention of the top-end plastic hinge formation at State-MCE

As shown in Fig. 2.4, in order to estimate the column bending moment at the State-MCE (Fig. 2.4a), the bending moment increment from State-UYM to State-MCE should be added to the bending moment at State-UYM, which is expressed by Eqn. 2.1. This increment is attributed to the strain hardening effect of the plastic hinges which had developed at State-UYM. For simplicity, it is assumed that the location of the plastic hinge forming at State-UYM is at the quarter column height. Solving the equation $M'(h_1/4) = 0$, the FSA top-end moment at State-UYM, $M_f = \omega_{ch1}h_1^2/4(1+\lambda)$ can be obtained. Then, the FSA shear force at State-UYM, V_f can be determined from $V_f = (1+\lambda)M_f/h_1 = \omega_{ch1}h_1^2/4$. This study introduces the overstrength factors Ω_f and Ω_p to account for the strain hardening of the boundary frame and infill plates at the state-MCE, respectively.

Thus, the incremental FSA shear force in the column from State-UYM to State-MCE is $\Delta V_{FSA} = (\Omega_f\text{-}1)V_f = (\Omega_f\text{-}1)\omega_{ch1}h_1^2/4$. Based on the assumption for the incremental FSA bending moment distribution shown in Fig. 2.4b, the incremental FSA top-end moment is $\Delta M_{FSA} = \Delta V_{FSA}\times(3h_1/4) = (3/16)(\Omega_f\text{-}1)\omega_{ch1}h_1^2$. On the other hand, Fig. 2.4c shows the incremental PFE bending moment distribution. It is assumed the magnitude of the PFE bending moment at State-MCE is Ω_p times that at State-PFE. The incremental PFE top-end moment is $\Delta M_{PFE} = (\Omega_p\text{-}1)\omega_{ch1}h_1^2/12$. Form the superposition of the top-end moment at State-UYM and incremental bending moments (ΔM_{PFE} and ΔM_{FSA}), the top-end moment

demand at State-MCE, $M^t_{d\text{-}MCE}$, can be obtained:

$$M^t_{d-MCE} = M_f + \frac{\omega_{ch1} h_1^2}{12} + \Delta M_{FSA} + \Delta M_{PFE} = \left[\frac{1}{4(1+\lambda)} + \frac{1}{12}\Omega_p + \frac{3}{16}(\Omega_f - 1) \right] \omega_{ch1} h_1^2 = \eta_2 \omega_{ch1} h_1^2 \quad (2.3)$$

The overturning axial force at the top end of the compressed bottom column at State-MCE can be determined based on the force diagrams shown in Fig. 2.3b incorporated with the strain hardening effects. The gravity load effect should be included in determining the total axial force demand $P^t_{d\text{-}MCE}$. If the reduced flexural strength of the column under the axial force $P^t_{d\text{-}MCE}$ is greater than $P^t_{d\text{-}MCE}$, it is guaranteed that the top-end plastic hinge will not form at State-MCE.

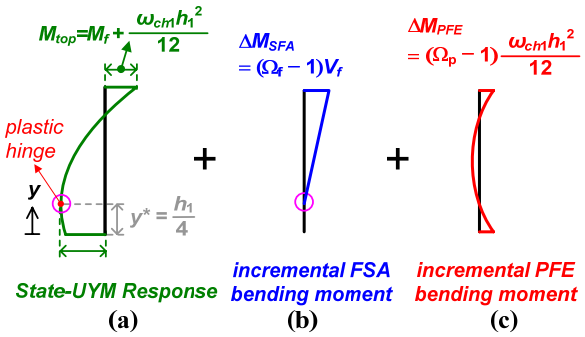

Figure 2.4. (a) Bending moment at State-UYM; (b) incremental FSA bending moment and (c) incremental PFE bending moment

3. EXPERIMETAL PROGRAM

3.1. Specimen design

There were three full-scale 2-story SPSW specimens in this experimental research. All three specimens had the same center-to-center line dimensions. The wall span was 3420 mm and each story height was 3820 mm (as shown in Fig. 3.1). All the steel plates were 2.7 mm thick low yield strength (LYS) steel with a measured yield stress, F_{yp} = 220 MPa. All the specimens adopted identical top beams (H400×200×10×14), middle beams (H300×150×10×12) and bottom beams (H400×200× 8×13). The key differences among these specimens are the sizes of the boundary columns. All the boundary elements were made of A572 grade 50 steel. The infill plates were welded at the edge to the boundary elements using 6 mm thick and 50 mm wide fishplate connection details. The continuous fishplates were welded to the beams and columns with fillet welds on both sides. Reduced beam sections details were adopted to deal with the beam-to-column connections for top beam and middle beam.

The three specimens are named NC (Normal Column), SC (Small Column) and WC (Weak Column). In the specimen design, the overstrength factors for the infill plate and boundary frame are assumed to be Ω_p = 1.1 and Ω_f = 1.2, respectively. It is assumed that the each boundary column is subjected to a gravity load $0.1P_y$ at the top level, where the P_y is the yield axial strength of the column. Table 3.1 lists the design check for the boundary columns for the three specimens considering the actual yield stresses of infill plate and frame members. The column (H320×310 ×16×25) in Specimen NC satisfies both of the proposed two design methods. This means that the bottom column top end would remain elastic at State-MCE (at a story drift of about 2.5% rad.). The column (H290×290×14×22) in Specimen SC satisfies the method 1 but does not satisfy the method 2. Its demand to capacity ratio (DCR) for method 2 is 1.04. The fact that the DCR is slightly greater than 1.0 suggests the bottom column top end could slightly yield at State-MCE. The column (H270×270×12×20) in Specimen WC satisfies neither of the proposed two methods. This represents that plastic hinge would form at the top end of the bottom column at State-UYM (about a story drift of 1% rad.).

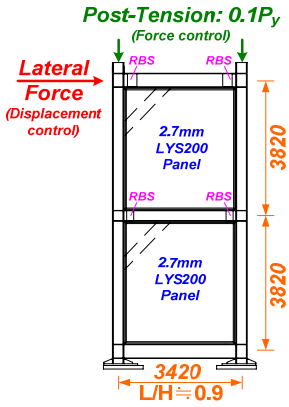

Figure 3.1. Configuration of the specimen

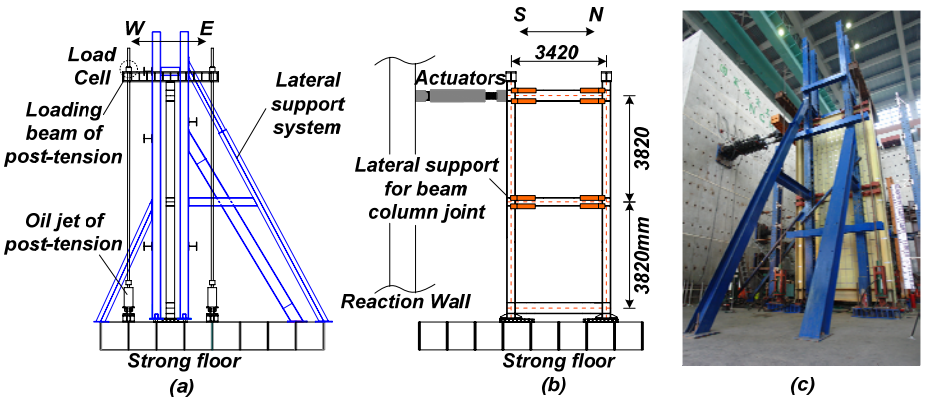

Figure 3.2. Test setup: (a) west-east elevation; (b) north-south elevation and (c) photo

Table 3.1. Design check for the columns

Specimen	Method 1		Method 2	
	P^b_d / P_y	$DCR = M_{p\text{-}req}/M_p^*$	$P^t_{d\text{-}MCE} / P_y$	$DCR = M^t_{d\text{-}MCE}/M_p^*$
NC	0.49	0.43 (O.K.)	0.39	0.57 (O.K.)
SC	0.61	0.83 (O.K.)	0.50	1.04 (N.G.)
WC	0.72	1.54 (N.G.)	0.58	1.72 (N.G.)

3.2. Test setup

Figure 3.2 shows the setup. A lateral support frame system was constructed in order to prevent the out-of-plane instability of the SPSW specimens. Special lateral support details were provided at the beam-to-column joints of the middle beams and the top beams such that the unbraced length of the columns is approximately equal to the typical height of one story.

Cyclically increasing displacements were applied onto the south column at the top beam elevation using two MTS243.70 actuators each with a stroke capacity of ±500mm and a force capacity of 980kN for tension and compression. Both two actuators were driven using the same displacement commands each corresponds to two cycles of positive and negative roof drift ratios of 0.1%, 0.25%, 0.5%, 0.75%, 1%, 1.5%, 2%, 2.5%, 3%, 4% and 4.5% rad. Before applying the cyclic lateral displacements, a vertical load of 10% of the column nominal axial yield capacity was applied at each column top using the post-tension rods. These vertical column loads were maintained during the test by using a hydraulic pressure stabilizing system.

4. TEST RESULTS

4.1. Force versus deformation relationships

Figure 4.1 shows the experimental cyclic force versus lateral drift relationships for the roof (top three figures), 2nd story and 1st story (lower three figures) of the three specimens. Since there was no concrete floor slab constructed in the specimens, horizontal boundary members were shortened under the panel tension field actions. Thus, the lateral displacements of the two vertical boundary elements were somewhat different, and the averages were used in calculating the responses shown in Figure 4.1. The peak experimental lateral forces were 1596kN, 1406kN and 1327kN for Specimens NC, SC and WC respectively. The analytical monotonic push-pull responses computed from the ABAQUS shell models are compared in Figure 4.1. It indicates that ABAQUS analyses predicted the overall nonlinear force versus deformation relationship of the three specimens very well. Detailed experimental observations are discussed in the following.

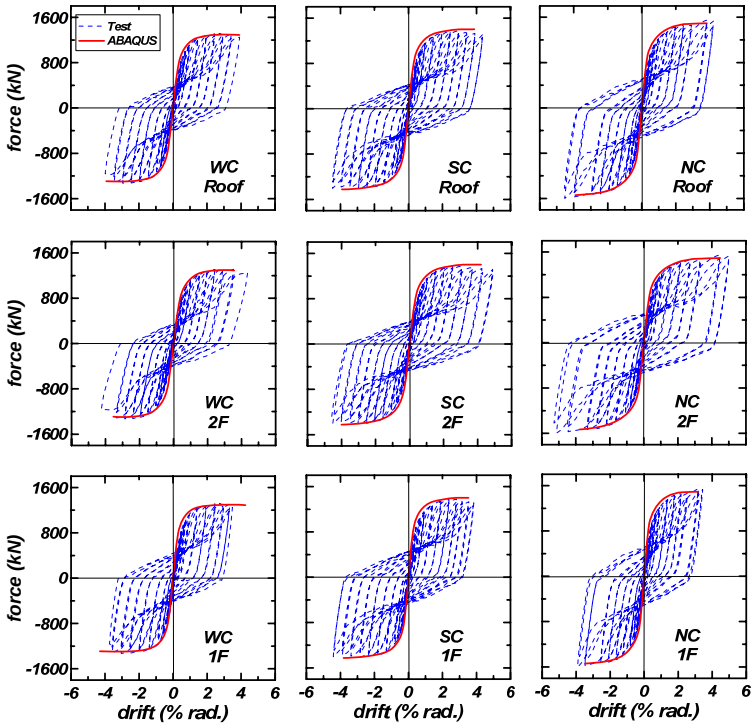

Figure 4.1. Experimental cyclic lateral drift versus force relationships and analytical pushover results

4.2. Observations of specimen responses

4.2.1. Specimen NC

The initial elastic stiffness of Specimen NC is about 43.5kN/mm. Specimen NC responded elastically when it was subjected to the cyclic roof drifts of 0.1% and 0.25% rad. without any flaking of whitewash. Buckling of the steel wall plates was observed when the roof drift reached 0.5% rad. At a roof drift of 0.75% rad., the beam flange yielded at the RBS locations. When the specimen was subjected the peak roof drifts of 1.0% and 1.5% rad. deformations, whitewash cracks were observable near the webs of the bottom column end and the bottom beam. At the roof drift of 1.5% rad., the cracks of whitewash on bottom columns were notable, extending 1500 mm from the bottom end up to an elevation between 1/4 to 1/2 of the column height. After the cyclic peak roof drift of 2.5% rad. was applied, web local buckling at RBSs in the top and middle beams was visible. Very slight whitewash flaking on the top ends of both two bottom columns was observed. Horizontal whitewash cracking lines were evident on the bottom column web from the bottom end to about 1/2 of the column height. Bottom column flange whitewash flaking was significant from the bottom end to slightly above 1/2 of the column height. Up to the two cyclic peak roof drifts of 4.5% rad. were completed, not much additional whitewashing flaking on the boundary elements was noticed.

4.2.2. Specimen SC

The initial elastic stiffness of Specimen SC is about 35.0kN/mm. Specimen SC responded elastically when it was subjected to the cyclic roof drifts of 0.1% and 0.25% rad. When the 0.75% rad. roof drift cycles were completed, uniform development of the tension field action of the infill plates was observed, and whitewash on the flanges of the bottom columns flaked uniformly from the base up to the half column height. The whitewash cracks at the RBS flanges were also observed. When the peak cyclic roof drifts of 1.0% and 1.5% rad. were applied, the whitewash flaking on the bottom column flanges grew from 1/2 to 3/4 of the column height. After the roof drift reached 2.5% rad., the bottom column flanges' whitewash flaking was very severe but did not extend into higher than 3/4 of the column height. Very slight whitewash cracks were found on the web near the top end of the bottom column. After the roof drift of 3.0% rad. was applied, slight lateral torsional buckling of the bottom column occurred, but the load-carrying capacity of the specimen is not deteriorated. Thus, test ended until the prescribed maximum roof drift of 4.5% rad. cycles were completed.

4.2.3. Specimen WC

The initial elastic stiffness of Specimen WC is about 33.4kN/mm. When the cyclic peak roof drift of 0.75% rad. was completed, whitewash flaked rather significantly in the flanges of the two bottom columns from 1/4 to 1/2 of the story height. The whitewash cracks at the RBS flanges were also observed. When the roof drifts of 1.0% and 1.5% rad. were applied, the flaking of whitewash on the bottom column flanges grew from 1/2 to 3/4 of the story height. Shear cracks of whitewash were observed in the webs of the two top ends of the bottom and top columns. When the peak roof drift first reached 2.0% rad., extensive shear cracks of the whitewash at the north bottom column top were evident, suggesting the formation of a plastic shear hinge. Very slight whitewash cracks were found on the web of the top end of the bottom column. After the peak roof drift reached 2.5% rad., significant lateral torsional buckling of the north column had occurred. Slight local buckling occurred at the RBSs. When the peak roof drift first reached 4.0% rad., yielding of the inner flanges of the 1st and 2nd story columns occurred. Whitewash flaked almost in the entire bottom columns. The lateral torsional buckling of the two columns became rather severe as shown. It has also caused the middle beam to bend in the out-of-plane direction. At this point, the strength of the Specimen WC had dropped notably. In order to prevent the damage of the lateral support system and the actuators, the test was terminated after applying only one complete cycle of 4.0% radians roof drift

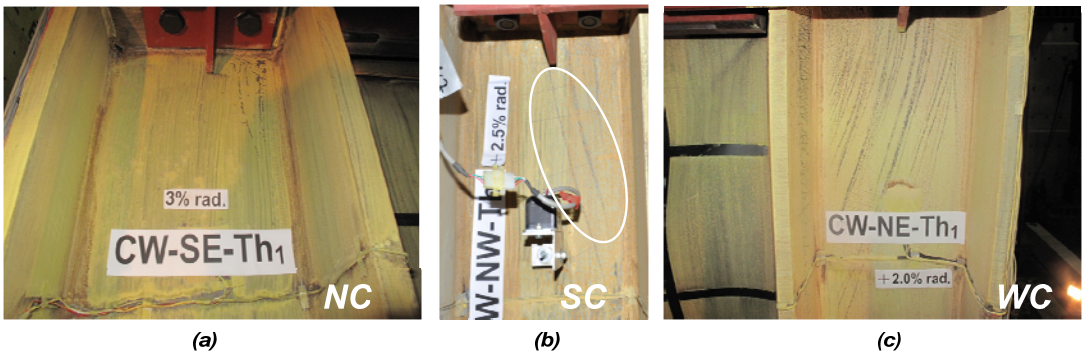

Figure 4.2. Conditions of the whitewashes at the top end of the columns in (a) Specimen NC (3% rad. roof drift); (b) Specimen SC (2.5% rad. roof drift) and (c) Specimen WC (2% rad. roof drift)

Figure 4.3. Conditions of the specimens after tests

4.3. Design implications from the tests

As shown in Fig. 4.2a, for specimen NC, the top ends of the 1st story columns remained elastic at a roof drift of 3.0% rad. For specimen SC, some slight flaking of whitewash was found at the top end of the 1st story column when the roof drift reached 2.5% rad. (Fig. 4.2b). For specimen WC, the yielding

of the top end of the 1st story column was initiated at a roof drift of 1% rad. As shown in Fig. 4.2c, the top end had yielded significantly at the 2% rad. roof drift level. The abovementioned responses at the top end of the 1st column agree with the predictions obtained from the proposed capacity design methods. These test results confirm the effectiveness of the proposed capacity design methods.

For specimens SC, the lateral torsional buckling (LTB) of the columns was initiated at the 3.0% rad. roof drift level. By contrast, significant LTB of columns in Specimen NC had occurred at a roof drift of 2.0% rad. It can be found that the occurrence of the column LTB was subsequent to the formation of the top-end plastic hinge in the 1st story column. Figure 4.3 shows the conditions of the specimens after the tests. It can be found that the columns in Specimen WC had significant permanent deformations. This suggests that the proposed design objective, which aims at preventing the occurrence of the top-end plastic hinge in the bottom column, is applicable.

5. CONCLUSIONS

This study proposes two capacity design methods for the bottom boundary column in SPSWs. One aims at preventing the yielding of the column top end prior to the plastic hinge formation in the lower half of the column when the plastic mechanism of the SPSW forms. The other intends to prevent the yielding of the column top end under MCE hazard level. Test results confirm the effectiveness of the proposed capacity designs. Test results also show that the occurrence of the top-end plastic hinge in the bottom column could result in the lateral torsional buckling of the boundary column. This confirms that the design objective in preventing the top-end plastic hinge is appropriate.

REFERENCES

American Institute of Steel Construction (AISC). (2010). AISC341-10: Seismic Provisions for Structural Steel Buildings. American Institute of Steel Construction (AISC), Chicago, Illinois, USA.

Berman, J.W., and Bruneau, M. (2003). Plastic analysis and design of steel plate shear walls. *Journal of Structural Engineering (ASCE).* **129: 11**, 1448-1456.

Berman, J.W., and Bruneau, M. (2008). Capacity design of vertical boundary elements in steel plate shear walls. *Engineering Journal (AISC)*. **15: 1**, 55-71.

Li, C.H., Tsai, K.C., Lin, C.H., and Chen, P.C. (2010). Cyclic tests of four two-story narrow steel plate shear walls. Part 2: experimental results and design implications. *Journal of Earthquake Engineering and Structural Dynamics*. **39: 7**, 801-826.

Li, C.H., Tsai, K.C., Lin, C.H., Chang, J.T., Lin, C.H., Chen, J.C., Lin, T.H. and Chen, P.C. (2011). Cyclic test of a substructural steel plate shear wall. *Journal of Earthquake Engineering and Structural Dynamics*. DOI: 10.1002/eqe.1180 (Early View).

Park, H.G., Kwack, J.H., Jeon, S.W., Kim, W.K., and Choi, I.R. (2007). Frame steel plate wall behavior under cyclic lateral loading. *Journal of Structural Engineering (ASCE)*. **133: 3**, 378-388.

Qu, B., Bruneau, M., Lin, C.H. and Tsai, K.C. (2008) Testing of Full Scale Two-Story Steel Plate Shear Wall with Reduced Beam Sections Connections and Composite Floors. *Journal of Structural Engineering (ASCE)*. **134: 3**, 364-373.

Qu, B. and Bruneau, M. (2010a). Capacity design of intermediate horizontal boundary elements of steel plate shear walls, *Journal of Structural Engineering (ASCE)*. **136: 6**, 665-675.

Qu, B. and Bruneau, M. (2010b). Behavior of vertical boundary elements in steel plate shear walls. *Journal of Engineering Journal (AISC)*. **47: 2**, 109-122.

Thorburn, L.J., Kulak, G.L. and Montgomery C.J. (1983). Analysis of Steel Plate Shear Walls, Structural Engineering Report No. 107, Dept. of Civil Engineering, Univ. of Alberta, Edmonton, Alberta, Canada.

Timler, P.A. and Kulak, G.L. (1983). Experimental Study of Steel Plate Shear Walls, Structural Engineering Report No. 114, Dept. of Civil Engineering, Univ. of Alberta, Edmonton, Alberta, Canada.

Tsai, K.C., Li, C.H., Lin, C.H., Tsai, C.Y. and Yu, Y.J. (2010). Cyclic tests of four two-story narrow steel plate shear walls. Part 1: analytical studies and specimen design. *Journal of Earthquake Engineering and Structural Dynamics*. **39: 7**, 775-799.

Vian, D., Bruneau, M., Tsai, K.C. and Lin, Y.C. (2009). Special perforated steel plate shear walls with reduced beam section anchor beams. I: experimental investigation**.** *Journal of Structural Engineering (ASCE)*. **135: 3**, 211-220.